Joint coding-denoising optimization of noisy images

Mikael Carlavan, Laure Blanc-Féraud, Marc Antonini, Carole Thiebaut, Christophe Latry and Yves Bobichon

Abstract

In this paper, we propose to study the problem of noisy source coding/denoising. This problem is challenging since a global optimization is usually difficult to perform as the global fidelity criterion needs to be optimized in the same time over the sets of both coding and denoising parameters. Most of the bibliography in this domain is based on the fact that, for a specific criterion, the global optimization problem can be simply separated into two independent optimization problems: The noisy image should be first optimally denoised and this denoised image should then be optimally coded. In many applications however, the layout of the acquisition imaging chain is fixed and cannot be changed, that is a denoising step cannot be inserted before coding. For this reason, we are concerned here with the problem of global joint optimization in the case the denoising step is performed, as usual, after coding/decoding. In this configuration, we show how to express the global distortion as a function of the coding and denoising parameters. We present then an algorithm to minimize this distortion and to get the optimal values of these parameters. We show results of this joint optimization algorithm on classical test images and on a high dynamic range image, visually and in a rate-distortion sense.

Index Terms

Global optimization, noisy source coding, quantizing, image denoising

M. Carlavan and L. Blanc-Féraud are with MORPHEME team, joint project between INRIA, CNRS and the University of Nice-Sophia Antipolis; M. Antonini is with I3S laboratory UMR7271 University of Nice Sophia-Antipolis and CNRS, CS 40121 - 06903 Sophia Antipolis, France (e-mail: carlavan@i3s.unice.fr, blancf@i3s.unice.fr, am@i3s.unice.fr).

C. Thiebaut and C. Latry are with CNES, 18 avenue Edouard Belin, 31401 Toulouse, France (e-mail: Carole.Thiebaut@cnes.fr, Christophe.Latry@cnes.fr).

Y. Bobichon is with Thales Alenia Space, 100 boulevard du Midi, 06156 Cannes la Bocca, France (e-mail: Yves.Bobichon@thalesaleniaspace.com).

I. Introduction

Images acquired by imaging systems are most of the time degraded by noise, which mainly comes from the imperfections of optical instruments. It is well-known that noise decreases the performances of coding schemes as it reduces the correlation between pixels [1]. This problem is commonly referred as the noisy source coding problem [2]. Many works have been devoted to address this issue [3], [4], [5], [6], [7], [8] and [9]. The majority of the mentioned works are based on the study of the global distortion optimization initially proposed by [5] and refined in [6]. This study states that the global distortion, if measured by the Mean Square Error (MSE), can be treated as two separated problems. First, the original source image should be optimally, in the minimum MSE sense, estimated from the noisy data and this estimate should then be optimally coded [6].

However, adding a supplementary step before coding is not always possible and in many cases the noisy acquired images are directly encoded without pre-processing. Critical applications such as satellite imaging can not indeed afford to insert pre-processing steps in the acquisition imaging chain as the on-board resources are highly limited. But one is still interested in optimizing the global imaging chain to obtain the best final image. So the imaging chain has to be considered as it is and the global distortion of this chain needs to be optimized. This is the focus of this paper.

More precisely, we are considering here the problem of optimal joint coding/denoising of a noisy image and focus on the acquisition imaging chain depicted Fig. 1. We show that, under certain hypotheses that we will describe, a closed-form expression of the global distortion can be obtained. We propose then to optimize this distortion, with respect to the coding and the denoising parameters, to reach the minimum global distortion. The originality of the proposed approach relies on the fact that we propose a global joint optimization which takes into account all the parameters of the imaging chain. We will also show that treating the optimization of coding/denoising as two separate problems (as in [7], [8], [9]) is suboptimal when the denoising is performed after coding. More precisely, we emphasize the necessity to take into account the denoising step in the rate-distortion allocation of the coder. And, as we will see, this requirement is confirmed by the results which display a significant improvement in comparison to the classical method which executes coding and denoising separately.

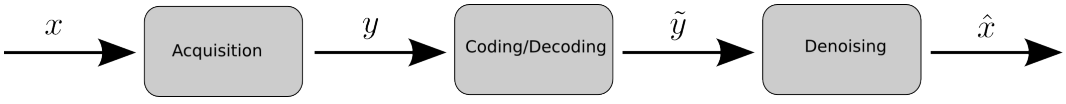

Fig. 1. Considered acquisition imaging chain.

The paper is organized as follows. Section II presents the studied imaging chain and introduces hypotheses and notations. In Section III, we detail the proposed approach and we show how to get a closed-form expression of the global distortion for the studied case. We detail the joint optimization of this distortion in Section IV and we present the algorithm to get the optimal parameters of the coding and the denoising steps. We show results, visually and in a rate-distortion sense, of the proposed joint optimization algorithm on classical test images and on a remote sensing image, in Section V. We conclude in Section VI and present perspectives for future works.

II. Hypotheses and notations

In the following, the operators applied to the image are denoted with a bold uppercase letter. The non-bold uppercase letters represent random variables whose realizations are denoted by a lowercase letter. With this notation, x is a realization of the random variable X. $(X)_i$ denotes the ith element of the random variable X. These variables are multidimensional $x \in \mathbb{R}^N$ where N is the number of pixels. W_x is a random variable associated to the wavelet transform of x and we denote $W_{x,j}, j \in \{0, \ldots, J-1\}$ (J being the number of subbands) the jth subband of the random variable W_x. We have $w_{x,j} \in \mathbb{R}^{N_j}$ where N_j is the size of the subband. Finally, we suppose that a wavelet subband $w_{x,j}$ follows a generalized centered Gaussian distribution law of parameter $\alpha_{w_{x,j}} > 0$ and variance $\sigma^2_{w_{x,j}} > 0$ [10]. A wavelet subband probability density function $p_{w_{x,j}}$ can then be modeled as

$$p_{w_{x,j}}(w_{x,j}) = \frac{A\left(\alpha_{w_{x,j}}\right)}{\sigma_{w_{x,j}}} e^{-\left|B\left(\alpha_{w_{x,j}}\right)\frac{w_{x,j}}{\sigma_{w_{x,j}}}\right|^{\alpha_{w_{x,j}}}}, \tag{1}$$

with

$$A\left(\alpha_{w_{x,j}}\right) = \frac{\alpha_{w_{x,j}} B\left(\alpha_{w_{x,j}}\right)}{2\Gamma\left(1/\alpha_{w_{x,j}}\right)} \tag{2}$$

$$B\left(\alpha_{w_{x,j}}\right) = \sqrt{\frac{\Gamma\left(3/\alpha_{w_{x,j}}\right)}{\Gamma\left(1/\alpha_{w_{x,j}}\right)}}, \tag{3}$$

and Γ is the usual Gamma function. The parameters $\sigma^2_{w_{x,j}}$ and $\alpha_{w_{x,j}}$ of the distribution law will be estimated using the kurtosis-based technique proposed in [11]. Note that the same assumption will be applied to all wavelet transforms in the chain with, of course, different distribution parameters.

As mentioned previously, we study the imaging chain shown Fig. 1. We consider the special case of coding techniques based on wavelet transforms [12], [13] and [14]. The coding step is then approximately decomposed in a non-redundant wavelet transform followed by a scalar subband quantizer. Note that this approximation is actually close to the coding schemes presented in the cited works.

We also consider that the denoising step is performed in the same wavelet basis than the coding. This choice may however need further explanations. Usually, an efficient wavelet transform for image denoising strongly differs from a wavelet transform suited for image coding. Image denoising techniques actually require redundant wavelet transforms to represent the characteristics of an image such as contours and oriented details while increasing the number of coefficients in image compression may be problematic [15]. Hence, a non-redundant wavelet transform used for image compression leads most of the time to poor denoising results. We are however very confident that using the same basis for both coding and denoising may provide a decoding-denoising structure gathered in a single fast and low resources algorithm. Extending the current work to complex denoising schemes such as [16] is a difficult task that will be addressed in future works.

Based on these considerations, the studied imaging chain is represented in detail Fig. 2.

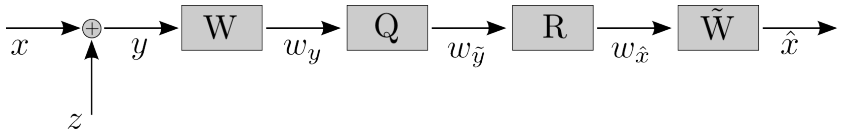

Fig. 2. Considered imaging chain

In this chain, we consider the instrumental noise z to be independent, identically distributed and to follow a centered normal distribution with variance σ_z^2. $\mathbf{W}$ is a wavelet transform, $\tilde{\mathbf{W}}$ its inverse. We denote $w_{x,j}$ and $w_{z,j}$ to be respectively the subband j of the wavelet transform of x and z. Each quantized subband $w_{\tilde{y},j}$ will be coded using an entropy encoder. As this operation does not introduce any degradation, it does not appear on the chain displayed figure 2. $\mathbf{R}$ is a linear restoration algorithm which operates independently on the wavelet coefficients of each subband j of the image and writes

$$w_{\hat{x},j} = \begin{array}{ll} \arg\min & \|w - w_{\tilde{y},j}\|_2^2 + \lambda_j \|w\|_2^2 \ , \\ \text{subject to} & w \in \mathbb{R}^{N_j} \end{array} \tag{4}$$

where $\lambda_j > 0$ is a regularizing parameter. The restoration algorithm (4) has a closed-form solution which writes

$$w_{\hat{x},j} = \frac{w_{\tilde{y},j}}{1 + \lambda_j}. \tag{5}$$

We are aware of the simplicity of the considered algorithm, it appears however that the linearity of the restoration algorithm $\mathbf{R}$ is required if one wants to write the global distortion in closed-form.

As mentioned previously, much work need to be addressed to consider the state-of-the-art denoising algorithms.

The quantizer $\mathbf{Q}$ is an infinite mid-tread scalar subband quantizer of step $\Delta_j > 0$ and is modeled as

$$\mathbf{Q}(w_{y,j}) = \Delta_j \left\lfloor \frac{w_{y,j}}{\Delta_j} + \frac{1}{2} \right\rfloor, \tag{6}$$

where $\lfloor \, \rfloor$ is the floor function which returns the greatest integer less than or equal to its argument. We now detail the basis of the proposed method to compute a closed-form expression of the global distortion.

Let $w_{b,j}$ be the coding error of the subband j

$$w_{b,j} = \mathbf{Q}(w_{y,j}) - w_{y,j}. \tag{7}$$

We have

$$\begin{aligned} w_{\tilde{y},j} = \mathbf{Q}(w_{y,j}) &= w_{y,j} + w_{b,j} \\ &= w_{x,j} + w_{z,j} + w_{b,j} \\ &= w_{x,j} + w_{\epsilon,j}, \end{aligned} \tag{8}$$

where $w_{\epsilon,j} = w_{z,j} + w_{b,j}$. The originality of the proposed method is to remark that the instrumental noise z can be explicitly used to decorrelate the first-order moments of the term $w_{\epsilon,j}$ to the ones of $w_{x,j}$, that is we consider that for any integer $m > 0$ and $n > 0$, we have

$$E\left[W_{\epsilon,j}^m W_{x,j}^n\right] = E\left[W_{\epsilon,j}^m\right] E\left[W_{x,j}^n\right], \tag{9}$$

where $W_{\epsilon,j}$ and $W_{x,j}$ are the random variables associated to $w_{\epsilon,j}$ and $w_{x,j}$. This hypothesis is mainly based on the fact that the quantizing part of the scheme Fig. 2 can be seen as a non-subtractive dithering system where the Gaussian instrumental noise acts as a dithering noise.

A dithering system consists in inserting a noise with a certain probability density function prior to quantizing, to improve the decorrelation property [17]. As mentioned in [18], a non-subtractive dithering system (named non-subtractive as the dithering noise is not substracted after quantizing) allows the moments of the global error (that is the sum of the coding error and dithering noise) to be fully decorrelated to the moments of the coding source.

It happens that a Gaussian distribution stands among the probability density functions which allow a noise to be considered as a dithering noise. The idea here is then to take benefit of the presence of the instrumental noise by considering it as a dithering noise. With such consideration, we know that the m first-order moments of the global error are decorrelated to the n first-order moments of the quantizing source [18], giving the property (9).

Moreover, if the instrumental noise z meets the dithering noise requirements, we also have [18]

$$E\left[W_{\epsilon,j}\right] = 0, \tag{10}$$

$$E\left[\|W_{\epsilon,j}\|^2\right] = N_j \sigma^2_{w_{z,j}} + N_j \frac{\Delta_j^2}{12}, \tag{11}$$

where $\sigma_{w_{z,j}}$ is the standard deviation of the distribution law of the wavelet transform $w_{z,j}$. From [17] we know that a Gaussian noise effectively owns the properties of a dither noise if the standard deviation of its distribution law is large enough. In the present case, the condition (9) will be verified if the following statement is true

$$\sigma_{w_{z,j}} > \frac{\Delta_j}{2}. \tag{12}$$

As the standard deviation of instrumental noise is usually low in imaging systems, the condition (12) assumes that the proposed approach will be valid only for high coding rate. We will however develop our method to consider all coding rates.

III. Global rate-distortion analysis

As mentioned in Section II, the studied imaging chain depends on two sets of parameters: The regularizing parameters λ_j in (5) and the quantizing steps Δ_j in (6), for each $j \in \{0, \ldots, J-1\}$. The global rate-distortion joint optimization problem consists in finding the optimal sets of parameters $\{\lambda_j^*\}$ and $\{\Delta_j^*\}$ which minimize the global distortion D under the constraint that the coding rate R does not exceed the target rate R_c. This can be formalized as the following

$$\begin{aligned} \{\lambda_j^*\}, \{\Delta_j^*\} = \quad & \arg\min \quad D(\{\lambda_j\}, \{\Delta_j\}) \\ & \text{subject to} \quad R(\{\lambda_j\}, \{\Delta_j\}) \leq R_c, \\ & \qquad\qquad \lambda_j > 0, j \in \{0, \ldots, J-1\} \\ & \qquad\qquad \Delta_j > 0, j \in \{0, \ldots, J-1\} \end{aligned} \quad . \tag{13}$$

Under this form, the optimization problem (13) is difficult to solve so that it is usually written under an unconstrained form [19]. Let $\tau > 0$ be a Lagrange mutliplier. The Lagrange dual function L writes

$$\begin{aligned} L(\tau) = \quad & \inf \quad D(\{\lambda_j\}, \{\Delta_j\}) + \tau \left(R(\{\lambda_j\}, \{\Delta_j\}) - R_c\right) \\ & \qquad \lambda_j > 0,\ j \in \{0, \ldots, J-1\} \\ & \qquad \Delta_j > 0,\ j \in \{0, \ldots, J-1\} \end{aligned} , \tag{14}$$

Problem (13) can then be written [20]

$$\{\lambda_j^*\}, \{\Delta_j^*\} = \max_{\tau > 0} L(\tau). \tag{15}$$

To solve the global distortion joint optimization problem (15), we need to express the global distortion D and the global coding rate R as a function of the regularizing parameters $\{\lambda_j\}$ and the quantizing steps $\{\Delta_j\}$.

Proposition 1: If $\sigma_{w_{z,j}}$ verifies hypothesis (12) for each $j \in \{0, \ldots, J-1\}$, then the global distortion D of the imaging chain displayed Fig. 2 writes

$$D(\{\lambda_j\}, \{\Delta_j\}) = \sum_{j=0}^{J-1} \frac{\pi_j a_j \lambda_j^2}{(1+\lambda_j)^2} \sigma^2_{w_{x,j}} + \frac{\pi_j a_j}{(1+\lambda_j)^2} \sigma^2_{w_{z,j}} + \frac{\pi_j a_j}{(1+\lambda_j)^2} \frac{\Delta_j^2}{12}, \tag{16}$$

where

$$a_j = \frac{N_j}{N}, \tag{17}$$

is the weight of the subband j in the whole image.

Proof: We start from the fact that the (mean) global distortion writes

$$D(\{\lambda_j\}, \{\Delta_j\}) = \frac{1}{N} E\left(\|X - \hat{X}\|^2\right), \tag{18}$$

where $\hat{X}$ is the random variable associated to the output final image $\hat{x}$. Thanks to the orthogonality of the wavelet subbands, the global distortion can also be formulated as

$$D(\{\lambda_j\}, \{\Delta_j\}) = \frac{1}{N} \sum_{j=0}^{J-1} \pi_j E\left(\|W_{x,j} - W_{\hat{x},j}\|^2\right), \tag{19}$$

where π_j are weighting coefficients which depend on the filters and the decimation factors used in the wavelet transform [21]. Note that these weighting coefficients are only required if one considers biorthogonal wavelet transforms such as the Cohen-Daubechies-Feauveau (CDF) 9/7 wavelet transform [22]. They are equal to 1 for an orthogonal wavelet transform.

In the case of the studied imaging chain displayed Fig. 2, the final image is the output of the restoration and writes

$$w_{\hat{x},j} = \mathbf{R} w_{\tilde{y},j}. \tag{20}$$

Using Eq. (5) and (8), the final image can be expressed as a function of the source and the global error

$$w_{\hat{x},j} = \frac{w_{x,j}}{1+\lambda_j} + \frac{w_{\epsilon,j}}{1+\lambda_j}. \tag{21}$$

From Eq. (19), (21) and using the moments decorrelation hypothesis (9), we deduce the global distortion

$$\begin{aligned} D(\{\lambda_j\}, \{\Delta_j\}) &= \frac{1}{N} E\left(\|X - \hat{X}\|^2\right) \\ &= \frac{1}{N} \sum_{j=0}^{J-1} \frac{\pi_j \lambda_j^2}{(1+\lambda_j)^2} E\left(\|W_{x,j}\|^2\right) + \frac{\pi_j}{(1+\lambda_j)^2} E\left(\|W_{\epsilon,j}\|^2\right). \end{aligned} \tag{22}$$

Finally, the global distortion (22) can be further developed using the results (11) to obtain the expression (16). ■

Note that the global distortion (16) requires the knowledge of the variance of each subband of the original image $\sigma^2_{w_{x,j}}$. This variance is generally unknown but can be roughly deduced from the observed image. For an orthogonal or a biorthogonal wavelet transform, the variance of the noise in each wavelet subband j is equal or almost equal (in the biorthogonal case) to the variance of the noise in the image domain, i.e. $\sigma^2_{w_{z,j}} = \sigma^2_z$, which is supposed to be known. Then, $\sigma^2_{w_{x,j}}$ can be computed during the rate-allocation of the coder from the observed subband variance $\sigma^2_{w_{y,j}}$ by

$$\sigma^2_{w_{x,j}} = \sigma^2_{w_{y,j}} - \sigma^2_z. \tag{23}$$

The second part of the problem (15) requires the expression of the global coding rate R. This rate can be expressed as the weighted sum of the rate in each subband R_j

$$R(\{\lambda_j\}, \{\Delta_j\}) = \sum_{j=0}^{J-1} a_j R_j(\Delta_j), \tag{24}$$

where a_j is given in (17). As mentioned in the hypotheses section, we assume that each quantized subband is encoded using an entropy encoder. The coding rate of a subband j can then be estimated by its entropy [23]

$$R_j(\Delta_j) = -\sum_{m=-\infty}^{+\infty} P_{w_{y,j}}(m, \Delta_j) \log_2 \left(P_{w_{y,j}}(m, \Delta_j) \right), \tag{25}$$

where $P_{w_{y,j}}(m, \Delta_j)$ is the probability to get the symbol m which depends on the density probability function $p_{w_{y,j}}$, defined in (1), of the subband $w_{y,j}$ and on the quantizing step Δ_j

$$P_{w_{y,j}}(m, \Delta_j) = \int_{m\Delta_j - \frac{\Delta_j}{2}}^{m\Delta_j + \frac{\Delta_j}{2}} p_{w_{y,j}}(w_{y,j}) dw_{y,j}. \tag{26}$$

As mentioned in the hypothesis section, we assume that each wavelet subband followed the generalized centered Gaussian distribution law defined in (1). The density probability function $p_{w_{y,j}}$ is then given by:

$$p_{w_{y,j}}(w_{y,j}) = \frac{A\left(\alpha_{w_{y,j}}\right)}{\sigma_{w_{y,j}}} e^{-\left| B(\alpha_{w_{y,j}}) \frac{w_{y,j}}{\sigma_{w_{y,j}}} \right|^{\alpha_{w_{y,j}}}}, \tag{27}$$

with

$$A\left(\alpha_{w_{y,j}}\right) = \frac{\alpha_{w_{y,j}} B\left(\alpha_{w_{y,j}}\right)}{2\Gamma\left(1/\alpha_{w_{y,j}}\right)} \tag{28}$$

$$B\left(\alpha_{w_{y,j}}\right) = \sqrt{\frac{\Gamma\left(3/\alpha_{w_{y,j}}\right)}{\Gamma\left(1/\alpha_{w_{y,j}}\right)}}, \tag{29}$$

and where $\sigma^2_{w_{x,j}}$ and $\alpha_{w_{x,j}}$ are the parameters of the distribution law, estimated using the kurtosis-based technique detailed in [11].

Proposition 2: The global rate-distortion optimization problem (13) can be solved by maximizing

$$L(\tau) = \begin{array}{ll} \inf & \phi_\tau(\{\lambda_j\},\{\Delta_j\}) \\ & \lambda_j > 0,\, j \in \{0,\dots,J-1\} \\ & \Delta_j > 0,\, j \in \{0,\dots,J-1\} \end{array}, \tag{30}$$

with respect to $\tau > 0$ and where

$$\phi_\tau(\{\lambda_j\},\{\Delta_j\}) = \sum_{j=0}^{J-1} \frac{\pi_j a_j \lambda_j^2}{(1+\lambda_j)^2}\sigma^2_{w_{x,j}} + \frac{\pi_j a_j}{(1+\lambda_j)^2}\sigma^2_{w_{z,j}} + \frac{\pi_j a_j \Delta_j^2}{12(1+\lambda_j)^2} + \tau\left(\sum_{j=0}^{J-1} a_j R_j(\Delta_j) - R_c\right). \tag{31}$$

Proof: This demonstration is straightforward. From Eq. (15), we define

$$\phi_\tau(\{\lambda_j\},\{\Delta_j\}) = D(\{\lambda_j\},\{\Delta_j\}) + \tau\left(R(\{\lambda_j\},\{\Delta_j\}) - R_c\right), \tag{32}$$

and we substitute D and R with their respective expressions (16) and (24). The reformulation of problem (13) is then obtained using equations (14) and (15). ■

We detail in the next part how to solve problem (13).

IV. Global rate-distortion optimization

Using proposition 2, the optimization problem (13) becomes

$$\{\lambda_j^*\},\{\Delta_j^*\} = \max_{\tau>0} \left(\begin{array}{ll} \inf & \phi_\tau(\{\lambda_j\},\{\Delta_j\}) \\ & \lambda_j > 0,\, j \in \{0,\dots,J-1\} \\ & \Delta_j > 0,\, j \in \{0,\dots,J-1\} \end{array} \right). \tag{33}$$

The existence and uniqueness of solutions of problem (33) is not straightforward but we can show that a solution of problem (33) exists and is unique (see Section VII). We propose a numerical algorithm to find this minimum. This algorithm is based on the resolution of the simultaneous equations obtained from the Karush-Kuhn-Tucker (KKT) conditions [24] of problem (33).

Proposition 3: The KKT conditions of problem (33) admits only one solution (λ_j^*, τ^*, Δ_j^*) which verifies

$$\lambda_j^* = \frac{\sigma^2_{w_{z,j}}}{\sigma^2_{w_{x,j}}} + \frac{{\Delta_j^*}^2}{12\sigma^2_{w_{x,j}}}. \tag{34}$$

$$\frac{\pi_j \Delta_j^*}{6(1+\lambda_j)^2} + \tau^* \frac{\partial R_j}{\partial \Delta_j}(\Delta_j^*) = 0. \tag{35}$$

$$\sum_{j=0}^{J-1} a_j R_j(\Delta_j^*) = R_c \tag{36}$$

Proof: From the KKT conditions of problem (33), we get $\forall j \in \{0, \ldots, J-1\}$ (see Section VII)

$$\begin{cases} \frac{\partial \psi(\lambda_j^*, \Delta_j^*, \tau^*)}{\partial \Delta_j} = \frac{a_j \pi_j \Delta_j^*}{6(1+\lambda_j^*)^2} + \tau^* a_j \frac{\partial R_j}{\partial \Delta_j}(\Delta_j^*) = 0, \\ \frac{\partial \psi(\lambda_j^*, \Delta_j^*, \tau^*)}{\partial \tau} = \sum_{j=0}^{J-1} a_j R_j(\Delta_j^*) - R_c = 0, \\ \frac{\partial \psi(\lambda_j^*, \Delta_j^*, \tau^*)}{\partial \lambda_j} = \frac{12 a_j \pi_j \lambda_j^* \sigma_{w_{x,j}}^2 - 12 a_j \pi_j \sigma_{w_{z,j}}^2 - a_j \pi_j {\Delta_j^*}^2}{6(1+\lambda_j^*)^3} = 0, \end{cases} \tag{37}$$

with

$$\frac{\partial R_j}{\partial \Delta_j}(\Delta_j) = -\frac{1}{\log(2)} \sum_{m=-\infty}^{+\infty} \left[1 + \log\left(P_{w_{y,j}}(m, \Delta_j)\right)\right] \times$$
$$\left[p_{w_{y,j}}\left(m\Delta_j + \frac{\Delta_j}{2}\right)\left(m + \frac{1}{2}\right) - p_{w_{y,j}}\left(m\Delta_j - \frac{\Delta_j}{2}\right)\left(m - \frac{1}{2}\right)\right], \tag{38}$$

and where

$$\psi(\{\lambda_j\}, \{\Delta_j\}, \tau) = \phi_\tau(\{\lambda_j\}, \{\Delta_j\}. \tag{39}$$

The expressions (34), (35) and (36) of the optimal parameters directly follow from the optimality conditions (37). The existence and uniqueness of these parameters is much longer and is addressed in Section VII. ■

As we can see from (34), (35) and (36), the parameters $\{\Delta_j^*\}$ and τ^* can not be computed analytically. But as mentioned in Section VII, any root-finding algorithms can be used to achieve this goal. For our simulations, binary search algorithms will be used for the computation of both $\{\Delta_j^*\}$, τ^* and for the sake of simplicity, each binary search algorithm will be parametrized to the same given precision $\rho = 0.1$.

The case of the low frequency subband ($j = J-1$) will be processed differently as we do not want to degrade these coefficients. We will only use quantizing to round these coefficients to their nearest integers. Consequently, we will set

$$\Delta_{J-1}^* = 1, \tag{40}$$

$$\lambda_{J-1}^* = \frac{\sigma_{w_{z,J-1}}^2}{\sigma_{w_{x,J-1}}^2} + \frac{1}{12\sigma_{w_{x,J-1}}^2}. \tag{41}$$

Finally, the overall joint optimization procedure for solving problem (13) is given in the Algorithm 1. Note that the binary search sub-procedures are not detailled in this process. Algorithm 1 intends to be quite general and we let the choice of the root-finding algorithms to the user.

Algorithm 1 Global rate-distortion joint optimization algorithm

Set $\tau = 1$, $\rho = 0.1$.

while $\left|\sum_{j=0}^{J-1} a_j R_j - R_c\right| > \rho$ **do**

for j from 0 to $J-2$ **do**

Set $\Delta_j = 1$ and compute the value of the regularizing parameter λ_j from (34).

while $\left|\frac{\pi_j \Delta_j}{6(1+\lambda_j)^2} + \tau \frac{\partial R_j}{\partial \Delta_j}(\Delta_j)\right| > \rho$ **do**

Increase the value of Δ_j and compute the value of the regularizing parameter λ_j from (34).

end while

end for

Set $\Delta_{J-1} = 1$ and compute the regularizing paramater λ_{J-1} from (41).

if $\left|\sum_{j=0}^{J-1} a_j R_j - R_c\right| > \rho$ **then**

Increase the value of τ.

end if

end while

Output the optimal parameters $\{\lambda_j^*\}$ and $\{\Delta_j^*\}$.

V. Results

We simulate the joint optimization algorithm 1 on the well-known test images *Lena*, *Barbara*, *Pirate* and on the high-dynamic range remote sensing image displayed Fig. 3.

For this simulation, we set the wavelet transform $\mathbf{W}$ to be a three levels CDF 9/7 wavelet transform [22] and $\mathbf{R}$ is given by (4). Each test image has been noised with an additive white Gaussian noise with a standard deviation σ_z equal to 15. As the efficiency of the proposed estimation depends on the standard deviation of this noise (see Eq. (12)), we simulate two more cases for the *Barbara* image: $\sigma_z = 5$ and $\sigma_z = 25$.

For each target rate, we simulate the imaging chain Fig. 2 with the usual disjoint optimization technique, which consists in selecting the quantizing steps and the regularizing parameters such that the coding and the restoration errors are independently minimized. The coding error minimization has been achieved using the rate-distortion allocation based model proposed in [25]. As for the restoration error, it has been minimized using an exhaustive search of the optimal regularizing parameters. Once the final image has

(a) (b)

(c) (d)

Fig. 3. Test images: (a) is *Lena* (256×256 pixels), (b) is *Barbara* (512×512 pixels), (c) is *Pirate* (1024×1024 pixels) and (d) is a high-dynamic range remote sensing image of Cannes harbour (12 bits, 30 cm resolution, 1024×1024 pixels).

been reconstructed using these parameters, we numerically compute the global distortion

$$D = \frac{1}{N}\|x - \hat{x}\|^2, \tag{42}$$

where x is the clean (i.e. noiseless) test image, assumed to be known in our numerical experiments, and $\hat{x}$ is the final image. The distortion (42) is the true distortion and will be referred as the ground truth in our simulations. The estimation model (16) of the global distortion that we proposed has then been computed with the values of parameters obtained for the ground truth. This allows to verify that the estimation (16) of the global distortion is close to the ground truth (42), implying the validity of

the proposed method. And finally, we use the proposed joint optimization algorithm 1 to compute the optimal parameters, that we inserted into the estimation model (16) to compute the minimal distortion.

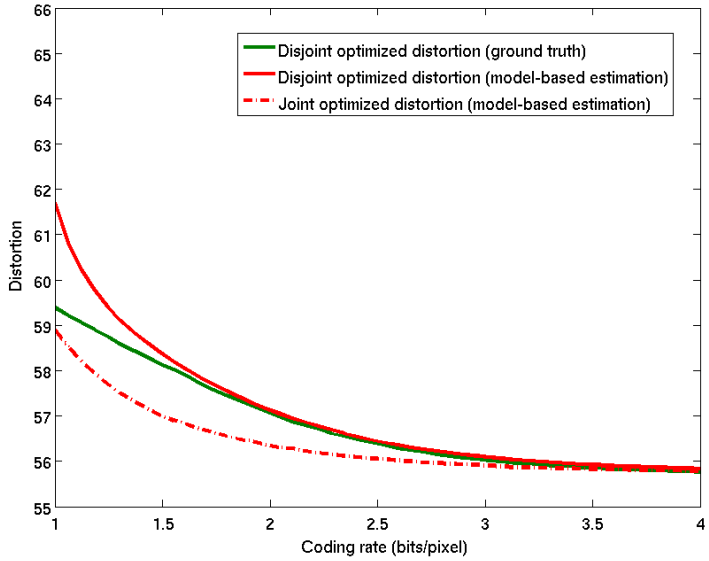

Fig. 4. Comparison of the disjoint optimized distortion (ground truth and model-based estimation) to the joint optimized distortion (model-based estimation) on *Lena*, $\sigma_z = 15$.

The resulting rate-distortion curves are given Fig. 4 to 8. We see that the validity of the proposed estimation, as expected by the hypothesis (12), is not always verified and depends on the target coding rate. More precisely, the proposed estimation approximates well the true distortion for medium to high coding rates but does not give satisfying results for low coding rates. This can be explained by the fact that for low coding rates, the condition (12) is not respected anymore and that the moments of the global error cannot consequently be considered decorrelated to the moments of the source. As mentioned previously, we performed several simulations on the *Barbara* image with different standard deviations of the noise such that the condition (12) can be verified for different ranges of coding rate. When the standard deviation is low (Fig. 5), we see that the proposed estimation is performant if the coding rate is around 2.5 bits/pixel and more. However for this high coding rate[1], the coding step is almost lossless such that the global optimization problem is reduced to the optimization of the restoration only. Therefore, the joint and the disjoint optimization techniques become the same and give then similar results.

[1]*Barbara* is originally encoded on 8 bits.

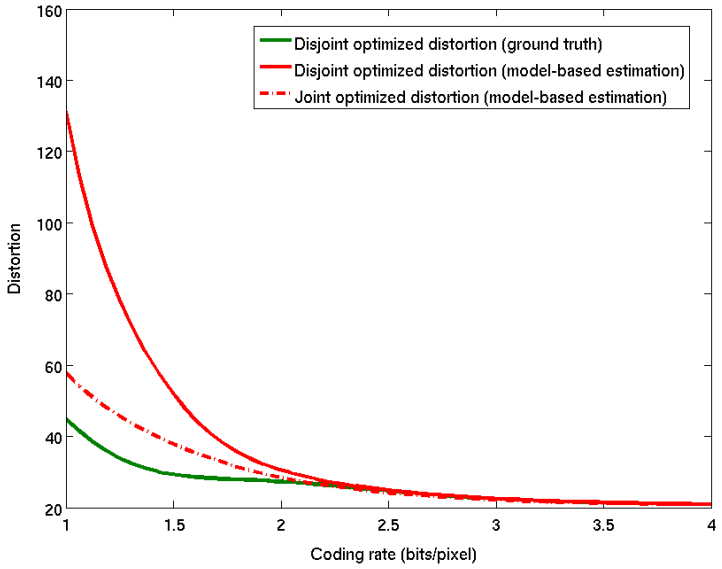

Fig. 5. Comparison of the disjoint optimized distortion (ground truth and model-based estimation) to the joint optimized distortion (model-based estimation) on *Barbara*, $\sigma_z = 5$.

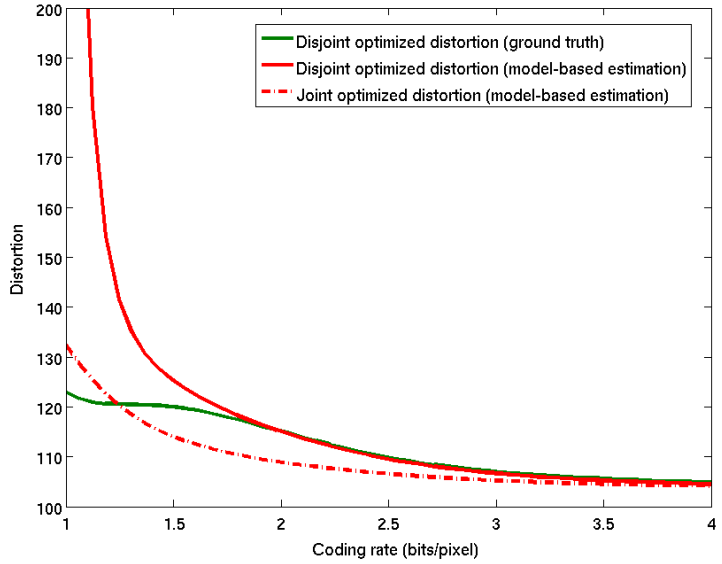

Fig. 6. Comparison of the disjoint optimized distortion (ground truth and model-based estimation) to the joint optimized distortion (model-based estimation) on *Barbara*, $\sigma_z = 15$.

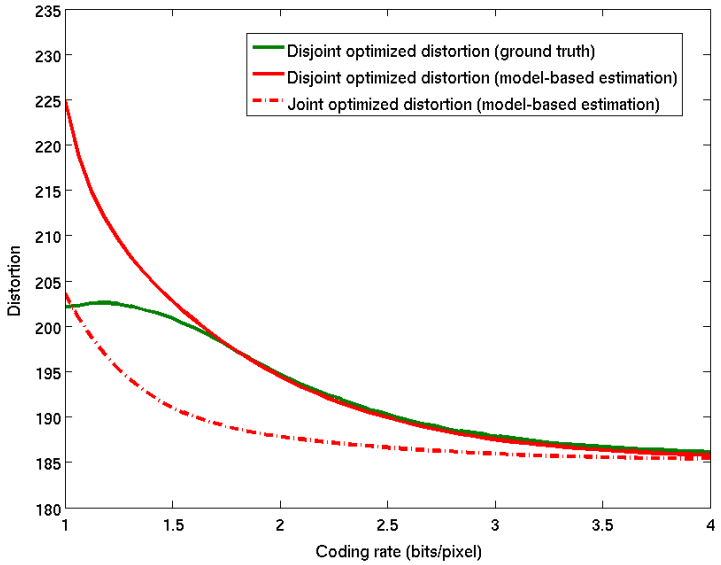

Fig. 7. Comparison of the disjoint optimized distortion (ground truth and model-based estimation) to the joint optimized distortion (model-based estimation) on *Barbara*, $\sigma_z = 25$.

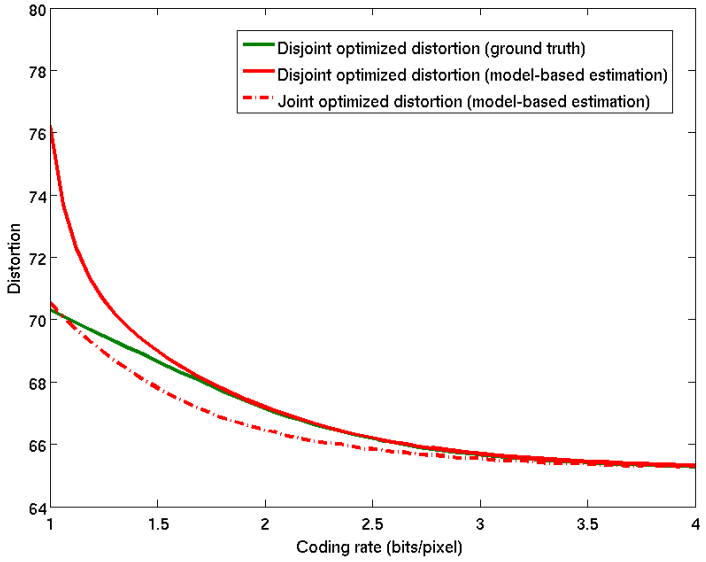

Fig. 8. Comparison of the disjoint optimized distortion (ground truth and model-based estimation) to the joint optimized distortion (model-based estimation) on *Pirate*, $\sigma_z = 15$.

As shown by Fig. 5, 6 and 7, the range of validity of the proposed estimation increases as the standard deviation increases. For a high standard deviation (Fig. 7), we can verify that the proposed estimation is valid for lower coding rates (around 1.8 bits/pixel and more). In that case, the joint optimization displays significant improvement in comparison to the disjoint optimization. It allows for example to reach the same global error than the disjoint optimized technique but for a lower coding rate. On the *Barbara* image and for $\sigma_z = 15$ (Fig. 6), the joint optimization technique reaches at 1.42 bits/pixel the same distortion than the one obtained at 2.04 bits/pixels for the disjoint optimization technique, saving therefore almost 30% of the bit budget. The benefit in term of compression performances of the joint optimization technique appears then to be very significant.

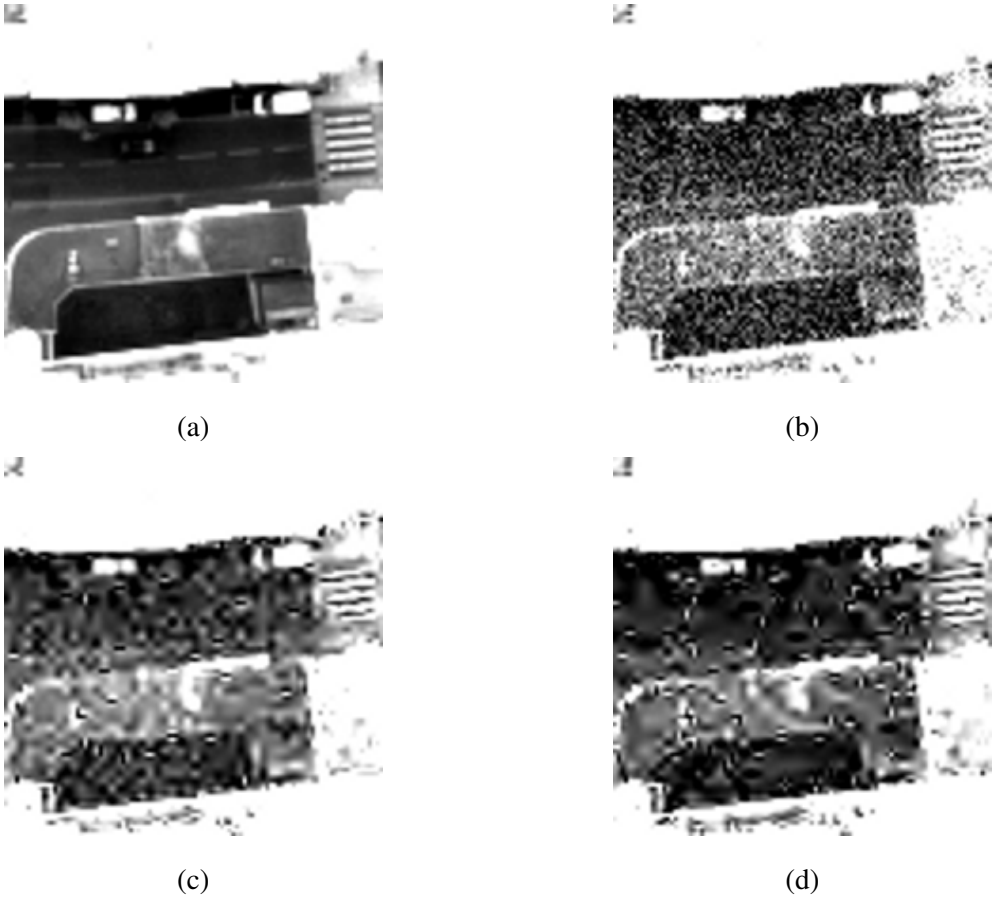

(a) (b) (c) (d)

Fig. 9. Visual comparison of reconstruction results. Displayed images have a size of 200×200 pixels. (a) is the reference image, (b) is the observed image, (c) is the image reconstructed with the parameters obtained by the disjoint minimization of the ground truth distortion and (d) is the image reconstructed with the parameters obtained by the joint optimization, performed using algorithm 1, of the estimated distortion. The coding rate is 2.5 bits/pixel. The image range has been extended to point up the image reconstruction artifacts.

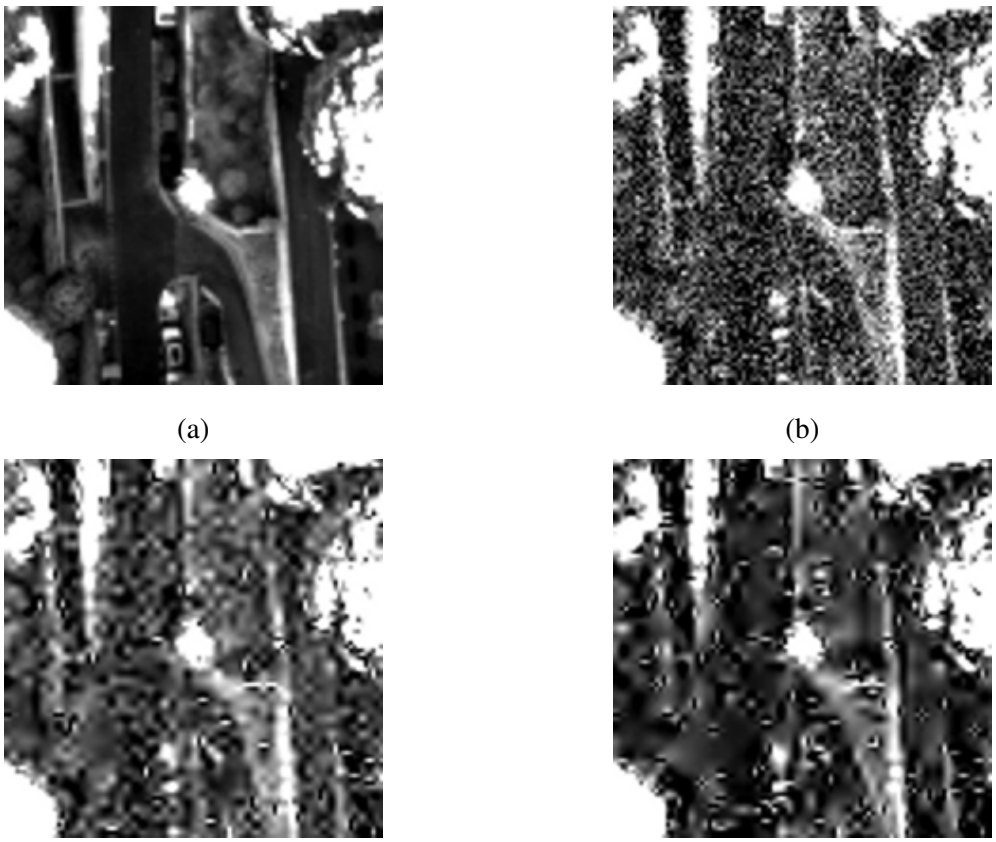

(a) (b)

(c) (d)

Fig. 10. Visual comparison of reconstruction results. Displayed images have a size of 200×200 pixels. (a) is the reference image, (b) is the observed image, (c) is the image reconstructed with the parameters obtained by the disjoint minimization of the ground truth distortion and (d) is the image reconstructed with the parameters obtained by the joint optimization, performed using algorithm 1, of the estimated distortion. The coding rate is 2.5 bits/pixel. The image range has been extended to point up the image reconstruction artifacts.

Visual results for the target rate of 2.5 bits/pixel are given Fig. 9 to 12 for the high-dynamic range remote sensing image. We do not focus on the quality of the reconstructed images regarding to the reference one as the considered chain is excessively simple. Clearly, the presence of artifacts on the reconstructed image is due to the simple hypothesis that we made on the restoration algorithm (4). On the contrary, we are more concerned on the improvement of the image quality of the joint optimized chain with respect to the disjoint optimized one. We can see that the global joint optimization of the chain always leads to a reconstructed image witch contains less blurry edges or ringing artifacts. This is particularly visible on the edges of the buildings Fig. 9 and 11. As mentioned in the introduction of this paper, the obtained results clearly point that optimizing coding and denoising separately is suboptimal.

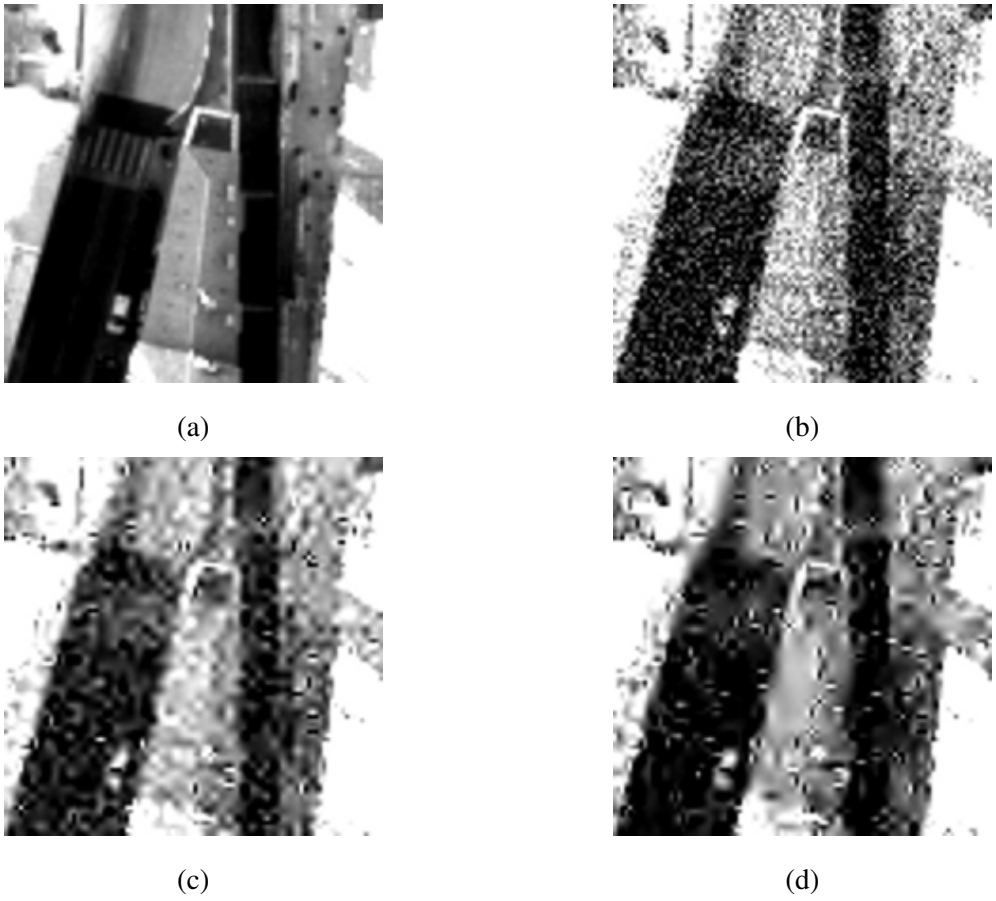

(a) (b)

(c) (d)

Fig. 11. Visual comparison of reconstruction results. Displayed images have a size of 200×200 pixels. (a) is the reference image, (b) is the observed image, (c) is the image reconstructed with the parameters obtained by the disjoint minimization of the ground truth distortion and (d) is the image reconstructed with the parameters obtained by the joint optimization, performed using algorithm 1, of the estimated distortion. The coding rate is 2.5 bits/pixel. The image range has been extended to point up the image reconstruction artifacts.

One needs instead to address the problem of imaging chain design in its globality; the proposed method and the obtained results are encouraging in this sense. A lot of works is however required to extend the proposed method to lower coding rates and to more complex denoising schemes.

VI. Conclusions

In this paper we considered the problem of joint noisy source coding/denoising. Most of the time, the coding and the denoising parameters are selected independently such that the coding and the restoration error are respectively minimized. This parameters selection technique leads however to a suboptimal distortion. It appears then crucial to address the problem of joint coding/denoising in its globality. We

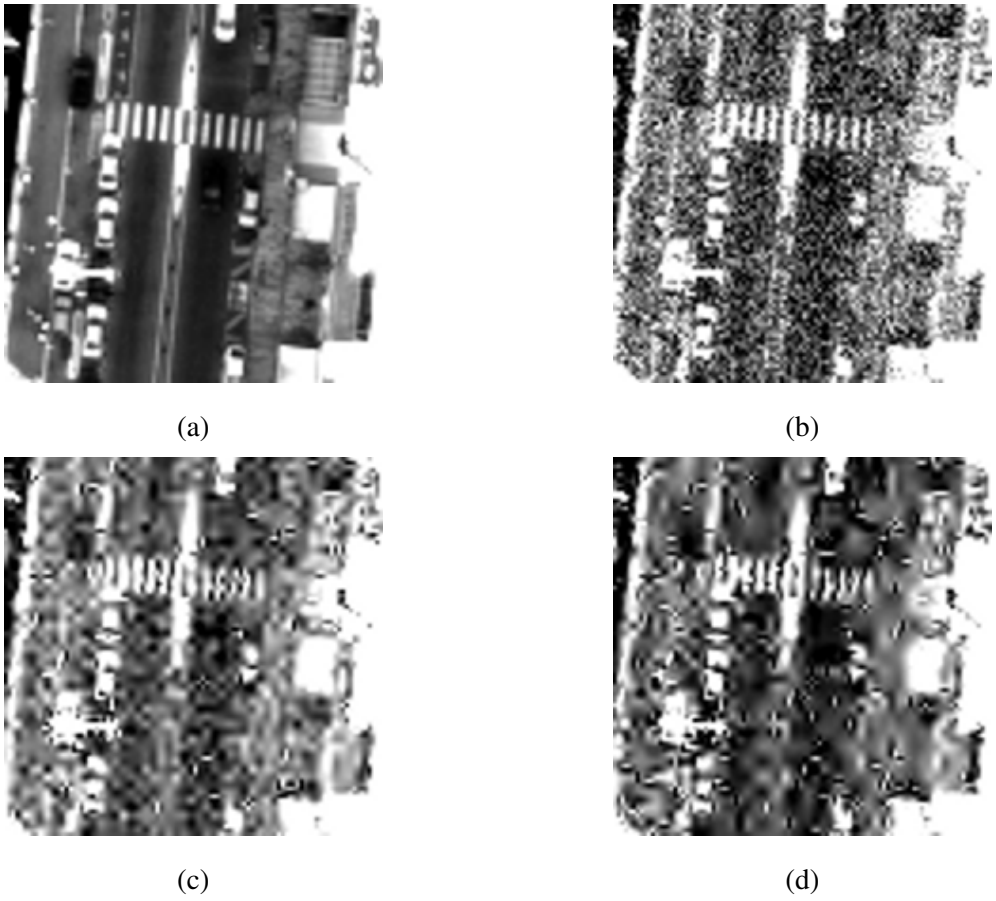

(a) (b)

(c) (d)

Fig. 12. Visual comparison of reconstruction results. Displayed images have a size of 200×200 pixels. (a) is the reference image, (b) is the observed image, (c) is the image reconstructed with the parameters obtained by the disjoint minimization of the ground truth distortion and (d) is the image reconstructed with the parameters obtained by the joint optimization, performed using algorithm 1, of the estimated distortion. The coding rate is 2.5 bits/pixel. The image range has been extended to point up the image reconstruction artifacts.

proposed here a technique to modelize the global distortion and we presented an algorithm to get the optimal coding and denoising parameters. We simulated this joint optimization technique on classical test images and on a high-dynamic range remote sensing image. We concluded that our joint coding/denoising optimization approach can either allows to reach the same quality at lower rates or to improve the quality of the reconstructed final image for the same rates, in comparison to the image obtained using the classical disjoint optimization technique. Further works will be focused on the extension of the proposed model to lower coding rates and to advanced denoising schemes.

VII. Existence and uniqueness of optimal parameters

We detail here the existence and uniqueness of optimal parameters of the following problem

$$\begin{aligned} \inf \quad & \phi_\tau(\{\lambda_j\},\{\Delta_j\}) \\ & \lambda_j > 0,\, \forall j \in \{0,\dots,J-1\} \\ & \Delta_j > 0,\, \forall j \in \{0,\dots,J-1\} \end{aligned} \quad , \tag{43}$$

where

$$\phi_\tau(\{\lambda_j\},\{\Delta_j\}) = \sum_{j=0}^{J-1} \frac{\pi_j a_j \lambda_j^2}{(1+\lambda_j)^2}\sigma^2_{w_{x,j}} + \frac{\pi_j a_j}{(1+\lambda_j)^2}\sigma_z^2 + \frac{\pi_j a_j \Delta_j^2}{12(1+\lambda_j)^2} + \tau\left(\sum_{j=0}^{J-1} a_j R_j(\Delta_j) - R_c\right). \tag{44}$$

To simplify the notations, we get rid of the constant R_c and the sum over j (as each subband is independent) in ϕ_τ, which now rewrites

$$\phi_\tau(\lambda_j,\Delta_j) = \frac{\pi_j a_j \lambda_j^2}{(1+\lambda_j)^2}\sigma^2_{w_{x,j}} + \frac{\pi_j a_j}{(1+\lambda_j)^2}\sigma_z^2 + \frac{\pi_j a_j \Delta_j^2}{12(1+\lambda_j)^2} + \tau a_j R_j(\Delta_j). \tag{45}$$

Proposition 4: Problem (43) admits an unique solution (λ_j^*,Δ_j^*) which verifies

$$\lambda_j^* = \frac{\sigma_z^2}{\sigma^2_{w_{x,j}}} + \frac{{\Delta_j^*}^2}{12\sigma^2_{w_{x,j}}} \tag{46}$$

$$\frac{\pi_j \Delta_j^*}{6(1+\lambda_j)^2} + \tau^* \frac{\partial R_j}{\partial \Delta_j}(\Delta_j^*) = 0 \tag{47}$$

Proof: To prove the existence and uniqueness of this solution, we propose to study the convexity of the function (45). We have

$$\frac{\partial \phi_\tau}{\partial \Delta_j}(\lambda_j,\Delta_j) = \frac{\pi_j a_j \Delta_j}{6(1+\lambda_j)^2} + \tau a_j \frac{\partial R_j}{\partial \Delta_j}(\Delta_j), \tag{48}$$

and

$$\frac{\partial^2 \phi_\tau}{\partial \Delta_j^2}(\lambda_j,\Delta_j) = \frac{\pi_j a_j}{6(1+\lambda_j)^2} + \tau a_j \frac{\partial^2 R_j}{\partial \Delta_j^2}(\Delta_j). \tag{49}$$

We also have

$$\begin{aligned} \frac{\partial \phi_\tau}{\partial \lambda_j}(\lambda_j,\Delta_j) &= \pi_j a_j \sigma^2_{w_{x,j}} \frac{\left(2\lambda_j(1+\lambda_j)^2 - 2(1+\lambda_j)\lambda_j^2\right)}{(1+\lambda_j)^4} - \pi_j a_j \sigma_z^2 \frac{2}{(1+\lambda_j)^3} \\ &\quad - \pi_j a_j \Delta_j^2 \frac{2}{12(1+\lambda_j)^3} \\ &= \pi_j a_j \left(\frac{12\lambda_j \sigma^2_{w_{x,j}} - 12\sigma_z^2 - \Delta_j^2}{6(1+\lambda_j)^3}\right) \end{aligned} \tag{50}$$

and

$$\frac{\partial^2 \phi_\tau}{\partial \lambda_j^2}(\lambda_j, \Delta_j) = \pi_j a_j \left(\frac{12\sigma^2_{w_{x,j}}}{6(1+\lambda_j)^3} - \frac{12\lambda_j \sigma^2_{w_{x,j}} - 12\sigma_z^2 - \Delta_j^2}{2(1+\lambda_j)^4} \right)$$
$$= \pi_j a_j \left(\frac{4\sigma^2_{w_{x,j}} - 8\lambda_j \sigma^2_{w_{x,j}} + 12\sigma_z^2 + \Delta_j^2}{2(1+\lambda_j)^4} \right) \quad (51)$$

Finally, we have

$$\frac{\partial^2 \phi_\tau}{\partial \lambda_j \partial \Delta_j}(\lambda_j, \Delta_j) = \frac{\partial^2 \phi_\tau}{\partial \Delta_j \partial \lambda_j}(\lambda_j, \Delta_j) = \frac{-a_j \pi_j \Delta_j}{3(1+\lambda_j)^3}. \quad (52)$$

Using (48) and (50), we deduce the expressions (46) and (47) of the solution $(\lambda_j^*, \Delta_j^*)$ which satisfies the first-order conditions

$$\frac{\partial \phi_\tau}{\partial \Delta_j}(\lambda_j^*, \Delta_j^*) = 0, \quad (53)$$

$$\frac{\partial \phi_\tau}{\partial \lambda_j}(\lambda_j^*, \Delta_j^*) = 0. \quad (54)$$

To ensure that this solution exists and is unique, we study the convexity of ϕ_τ through its Hessian matrix H_{ϕ_τ}, which writes

$$H_{\phi_\tau}(\lambda_j, \Delta_j) = \begin{bmatrix} \frac{\partial^2 \phi_\tau}{\partial \Delta_j^2}(\lambda_j, \Delta_j) & \frac{\partial^2 \phi_\tau}{\partial \Delta_j \partial \lambda_j}(\lambda_j, \Delta_j) \\ \frac{\partial^2 \phi_\tau}{\partial \lambda_j \partial \Delta_j}(\lambda_j, \Delta_j) & \frac{\partial^2 \phi_\tau}{\partial \lambda_j^2}(\lambda_j, \Delta_j) \end{bmatrix}. \quad (55)$$

Since H_{ϕ_τ} is a 2×2 matrix, we conclude from [28] that the function ϕ_τ is strictly convex if

$$\frac{\partial^2 \phi_\tau}{\partial \Delta_j^2}(\lambda_j, \Delta_j) > 0, \quad (56)$$

$$\frac{\partial^2 \phi_\tau}{\partial \lambda_j^2}(\lambda_j, \Delta_j) > 0, \quad (57)$$

and if the determinant of H_{ϕ_τ} is strictly positive

$$\det\left(H_{\phi_\tau}(\lambda_j, \Delta_j)\right) = \frac{\partial^2 \phi_\tau}{\partial \Delta_j^2}(\lambda_j, \Delta_j) \frac{\partial^2 \phi_\tau}{\partial \lambda_j^2}(\lambda_j, \Delta_j) - \left(\frac{\partial^2 \phi_\tau}{\partial \Delta_j \partial \lambda_j}(\lambda_j, \Delta_j) \right)^2 > 0. \quad (58)$$

The coding rate R_j is a monotonically decreasing positive function with respect to Δ_j [26], Δ_j being positive. Its limits are zero when Δ_j tends to infinity and infinity when Δ_j vanishes to zero [27]. Its derivative $\frac{\partial R_j}{\partial \Delta_j}$ is negative and monotonically increasing, whose limits are minus infinity when Δ_j vanishes to zero and zero when Δ_j tends to infinity [26]. Still from [26], we have that $\frac{\partial^2 R_j}{\partial \Delta_j^2}$ is positive and monotonically decreasing. Since τ is positive, we deduce from (49) that

$$\frac{\partial^2 \phi_\tau}{\partial \Delta_j^2}(\lambda_j, \Delta_j) > 0, \quad \forall (\Delta_j, \lambda_j) \quad (59)$$

From equation (51), it is clear that $\frac{\partial^2\phi_\tau}{\partial\lambda_j^2}$ is not always positive and we have

$$\frac{\partial^2\phi_\tau}{\partial\lambda_j^2}(\lambda_j,\Delta_j)\begin{cases}>0, & \text{if } 0<\lambda_j<\lambda_j^h\\ =0, & \text{if } \lambda_j=\lambda_j^h\\ <0, & \text{otherwise,}\end{cases} \tag{60}$$

with

$$\lambda_j^h=\frac{1}{2}+\frac{12\sigma_z^2+\Delta_j^2}{8\sigma_{w_{x,j}}^2}=\frac{1}{2}+\frac{3}{2}\lambda_j^*. \tag{61}$$

We need now to compute the determinant of the Hessian matrix H_{ϕ_τ}. Let us assume that $\frac{\partial^2\phi_\tau}{\partial\lambda_j^2}(\lambda_j,\Delta_j)$ is strictly positive and let us define

$$g(\lambda_j,\Delta_j)=\frac{\pi_j a_j}{6(1+\lambda_j)^2}\frac{\partial^2\phi_\tau}{\partial\lambda_j^2}(\lambda_j,\Delta_j)-\frac{a_j^2\pi_j^2\Delta_j^2}{9(1+\lambda_j)^6}. \tag{62}$$

Using equations (58) and (62), we have

$$\det\left(H_{\phi_\tau}(\lambda_j,\Delta_j)\right)=g(\lambda_j,\Delta_j)+\tau a_j\frac{\partial^2 R_j}{\partial\Delta_j^2}(\Delta_j)\frac{\partial^2\phi_\tau}{\partial\lambda_j^2}(\lambda_j,\Delta_j) \tag{63}$$

Since $\tau a_j\frac{\partial^2 R_j}{\partial\Delta_j^2}(\Delta_j)$ is always strictly positive, we get the following inequality

$$\det\left(H_{\phi_\tau}(\lambda_j,\Delta_j)\right)>g(\lambda_j,\Delta_j), \tag{64}$$

such that if $g(\lambda_j,\Delta_j)>0$ then we directly deduce that the Hessian matrix H_{ϕ_τ} is strictly positive and thus the function ϕ_τ is strictly convex. We have

$$\begin{aligned}g(\lambda_j,\Delta_j)&=\left(\frac{\pi_j^2a_j^2}{6(1+\lambda_j)^2}\right)\left(\frac{4\sigma_{w_{x,j}}^2-8\lambda_j\sigma_{w_{x,j}}^2+12\sigma_z^2+\Delta_j^2}{2(1+\lambda_j)^4}\right)-\frac{a_j^2\pi_j^2\Delta_j^2}{9(1+\lambda_j)^6}\\&=\frac{\pi_j^2a_j^2}{3}\left(\frac{12\sigma_{w_{x,j}}^2-24\lambda_j\sigma_{w_{x,j}}^2+36\sigma_z^2-\Delta_j^2}{12(1+\lambda_j)^6}\right).\end{aligned} \tag{65}$$

From (65), we can conclude that $g(\lambda_j,\Delta_j)>0$ if

$$12\sigma_{w_{x,j}}^2-24\lambda_j\sigma_{w_{x,j}}^2+36\sigma_z^2-\Delta_j^2>0, \tag{66}$$

that is, if

$$\lambda_j<\lambda_j^c, \tag{67}$$

where

$$\lambda_j^c=\frac{1}{2}+\frac{3}{2}\frac{\sigma_z^2}{\sigma_{w_{x,j}}^2}-\frac{\Delta_j^2}{24\sigma_{w_{x,j}}^2}. \tag{68}$$

Since $\lambda_j^c < \lambda_j^h$, we have from (60)

$$\frac{\partial^2 \phi_\tau}{\partial \lambda_j^2}(\lambda_j, \Delta_j) > 0, \quad \forall \Delta_j \,\text{and}\, \forall \lambda_j < \lambda_j^c, \tag{69}$$

which confirms the positivity hypothesis used to get inequality (64). We deduce that

$$\det\left(H_{\phi_\tau}(\lambda_j, \Delta_j)\right) > 0, \quad \forall (\lambda_j, \Delta_j) \in]0, \lambda_j^c[\times\mathbb{R}_+^*. \tag{70}$$

We can thus conclude that the function ϕ_τ is only convex locally on the convex domain $]0, \lambda_j^c[\times\mathbb{R}_+^*$.

From now, we set Δ_j to be equal to the optimal value Δ_j^*. Let us imagine that $\lambda_j^* > \lambda_j^c$, then we get that

$$\begin{aligned}
\frac{\sigma_z^2}{\sigma_{w_{x,j}}^2} + \frac{\Delta_j^{*2}}{12\sigma_{w_{x,j}}^2} &> \frac{1}{2} + \frac{3}{2}\frac{\sigma_z^2}{\sigma_{w_{x,j}}^2} - \frac{\Delta_j^{*2}}{24\sigma_{w_{x,j}}^2} \\
\frac{3\Delta_j^{*2}}{12\sigma_{w_{x,j}}^2} &> \frac{1}{2}\frac{\left(\sigma_z^2 + \sigma_{w_{x,j}}^2\right)}{\sigma_{w_{x,j}}^2} \\
\Delta_j^{*2} &> 2\left(\sigma_z^2 + \sigma_{w_{x,j}}^2\right),
\end{aligned} \tag{71}$$

which is non-sense as it means that the optimal quantizing step would be greater than the standard deviation of the signal to quantize. In particular, note that $+\infty$ also verifies (71) although it completely cancels the signal. Condition (71) is also contradictory to the dithering hypothesis (12) that we made to develop our method, which comforts ourselves that this behavior never happens and that we always have $\lambda_j^* < \lambda_j^c$. This result suggests that the point $(\lambda_j^*, \Delta_j^*)$ always lie in the strictly convex part of the function ϕ_τ.

If the evaluate $\frac{\partial^2 \phi_\tau}{\partial \lambda_j^2}$ at the point $(\lambda_j^*, \Delta_j^*)$, we have from (60) and using the fact that $\lambda_j^* < \lambda_j^h$ (see 61)

$$\frac{\partial^2 \phi_\tau}{\partial \lambda_j^2}(\lambda_j^*, \Delta_j^*) > 0. \tag{72}$$

Using (59), (70), (72) and [28], we deduce that the solution $(\lambda_j^*, \Delta_j^*)$ is a strict local minimum of the function ϕ_τ. If we look further at (48), we have

$$\frac{\partial \phi_\tau}{\partial \lambda_j}(\lambda_j, \Delta_j^*) \begin{cases} > 0, & \text{if } \lambda_j > \lambda_j^* \\ = 0, & \text{if } \lambda_j = \lambda_j^* \\ < 0, & \text{otherwise.} \end{cases} \tag{73}$$

The derivative is strictly positive for any $\lambda_j > \lambda_j^*$, we deduce that

$$\phi_\tau(\lambda_j, \Delta_j^*) > \phi_\tau(\lambda_j^*, \Delta_j^*), \quad \forall \lambda_j > \lambda_j^*. \tag{74}$$

Since ϕ_τ is strictly convex on the domain $]0, \lambda_j^c[\times\mathbb{R}_+^*$ whose strict local minimum is λ_j^*, we deduce

$$\phi_\tau(\lambda_j, \Delta_j) > \phi_\tau(\lambda_j^*, \Delta_j^*), \quad \forall \Delta_j \,\text{and}\, \forall \lambda_j \quad \text{with } 0 < \lambda_j < \lambda_j^c \quad \text{and}\, \lambda_j \neq \lambda_j^*. \tag{75}$$

Using (74) and (75), we have

$$\phi_\tau(\lambda_j, \Delta_j) > \phi_\tau(\lambda_j^*, \Delta_j^*) \quad \forall \Delta_j \,\text{and}\, \forall \lambda_j > 0 \quad \text{with}\, \lambda_j \neq \lambda_j^*, \tag{76}$$

which concludes that the solution $(\lambda_j^*, \Delta_j^*)$ is the unique global minimum of the function ϕ_τ. ■

We now have to deal with the numerical computation of the optimal parameters. Since the optimal regularizing parameter λ_j^* is expressed in closed-form, its computation is straightforward. The computation of the optimal quantizing step Δ_j^* is not direct as, for a given $\tau > 0$, we need to find a root of

$$g_\tau(\Delta) = \frac{\pi_j \Delta_j}{6\left(1 + \frac{\sigma^2_{w_{z,j}}}{\sigma^2_{w_{x,j}}} + \frac{{\Delta_j}^2}{12\sigma^2_{w_{x,j}}}\right)^2} + \tau \frac{\partial R_j}{\partial \Delta_j}(\Delta_j). \tag{77}$$

The monotony of the function g_τ is not easy to study since the term $\frac{\partial R_j}{\partial \Delta_j}$ is complex to evaluate. From our numerical experiments, we found out that the optimal quantizing step Δ_j^* always lies on a monotonically increasing part of the function g_τ. From this observation, we propose to use a binary search algorithm to compute this parameter. From (77), we see that Δ_j^* is function of τ. It seems reasonable to think that the higher τ is, the higher Δ_j^* needs to be for the function (77) to cross zero. This implies that the optimal quantizing step Δ_j^* can then be noted as a function of τ

$$\Delta_j^* = f(\tau), \tag{78}$$

where f is an increasing function. Consequently, from [26], we deduce that the coding rate R_j is a monotonically decreasing function with respect to τ. Using (36) and (78), we define

$$h(\tau) = \sum_{j=0}^{J-1} a_j R_j(f(\tau)) - R_c. \tag{79}$$

Then it seems clear that the function h is a monotonically decreasing function with respect to τ whose limits are infinity when τ vanishes to zero and $-R_c$ when τ tends to infinity. Its root τ^*, which verifies $h(\tau^*) = 0$, can then be computed using any root-finding algorithm.

REFERENCES

[1] S.-C.B. Lo, B. Krasner, S.K. Mun. Noise impact on error-free image compression. *IEEE Transactions on Medical Imaging*, 9(2):202–206, 1990.

[2] R. Dobrushin, B. Tsybakov Information transmission with additional noise. *IEEE Transactions on Information Theory*, 8(5):293–304, 1962.

[3] E. Ayanoglu. On optimal quantization of noisy sources. *IEEE Transactions on Information Theory*, 36(6)1450–1452, 1990.

[4] Y. Ephraim, R.M. Gray. A unified approach for encoding clean and noisy sources by means of waveform and autoregressive model vector quantization. *IEEE Transactions on Information Theory*, 34(4):826–834, 1988.

[5] D. Sakrison. Source encoding in the presence of random disturbance. *IEEE Transactions on Information Theory*, 14(1):165–167, 1968.

[6] J. Wolf, J. Ziv. Transmission of noisy information to a noisy receiver with minimum distortion. *IEEE Transactions on Information Theory*, 16(4):406–411, 1970.

[7] D. Rebollo-Monedero, S. Rane, B. Girod. Wyner-Ziv quantization and transform coding of noisy sources at high rates. *Asilomar Conference on Signals, Systems and Computers*, 2(1):2084–2088, 2004.

[8] T.R. Fischer, J.D. Gibson, B. Koo. Estimation and noisy source coding. *IEEE Transactions on Acoustics, Speech and Signal Processing*, 38(1):23–34, 1990.

[9] O.K. Al-Shaykh, R.M. Mersereau. Lossy compression of noisy images. *IEEE Transactions on Image Processing*, 7(12):1641–1652, 1998.

[10] M. Antonini, M. Barlaud, P. Mathieu, P. and I. Daubechies. Image coding using wavelet transform. *IEEE Transactions on Image Processing*, 1(2):205–220, 1992.

[11] J.H. Kasner, M.W. Marcellin, B.R Hunt. Universal trellis coded quantization. *IEEE Transactions on Image Processing*, 8(12):1677–1687, 1999.

[12] J.M Shapiro. Embedded image coding using zerotrees of wavelet coefficients. *IEEE Transactions on Signal Processing*, 41(12):3445–3462, 1993.

[13] A. Said and W.A. Pearlman. A new, fast, and efficient image codec based on set partitioning in hierarchical trees. *IEEE Transactions on Circuits and Systems for Video Technology*, 6(3):243–250, 1996.

[14] D. Taubman. High performance scalable image compression with EBCOT. *IEEE Transactions on Image Processing*, 9(7):1158–1170, 2000.

[15] V. Chappelier and C. Guillemot. Oriented Wavelet Transform for Image Compression and Denoising. *IEEE Transactions on Image Processing*, 15(10):2892–2903, 2006.

[16] D.L. Donoho. De-noising by soft-thresholding. *IEEE Transactions on Information Theory*, 41(3):613–627, 1995.

[17] J. Vanderkooy, S.P. Lipshitz. Dither in Digital Audio. *Journal of the Audio Engineering Society*, 35(12):966–975, 1987.

[18] R.A. Wannamaker, S.P. Lipshitz, J. Vanderkooy, J.N. Wright. A theory of nonsubtractive dither. *IEEE Transactions on Signal Processing*, 48(2):499–516, 2000.

[19] H. Everett. Generalized Lagrange Multiplier Method for Solving Problems of Optimum Allocation of Resources. *Operations Research*, 11(3):399–417, 1963.

[20] S. Boyd, L. Vandenberghe. Convex Optimization. *Cambridge University Press*, New York, USA, 2004.

[21] B. Usevitch. Optimal bit allocation for biorthogonal wavelet coding. *Data Compression Conference*, 387–395, 1996.

[22] A. Cohen, I. Daubechies, J.-C. Feauveau. Biorthogonal bases of compactly supported wavelets. *Communications on Pure and Applied Mathematics*, 45(5):485–560, 1992.

[23] C.E. Shannon. A Mathematical Theory of Communication. *Bell System Technical Journal*, 27(3):379–423, 1948.

[24] H.W. Kuhn, A.W. Tucker. Nonlinear programming. *Berkeley Symposium on Mathematical Statistics and Probability*, 481–492, 1951.

[25] C. Parisot, M. Antonini, M. Barlaud, S. Tramini, C. Latry and C. Lambert-Nebout. Optimization of the Joint Coding/decoding Structure. *IEEE International Conference on Image Processing*, 2001.

[26] C.E. Shannon. Coding theorems for a discrete source with a fidelity criterion. *IRE International Convention Record*, 7:142–163, 1959.

[27] H. Gish, J. Pierce. Asymptotically efficient quantizing. *IEEE Transactions on Information Theory*, 14(5):676–683, 1968.

[28] R.T. Rockafellar Convex Analysis. *Princeton Mathematical Series*, 1997.